REPORT DOCUMENTATION PAGE

Form Approved OMB NO. 0704-0188

1. REPORT DATE (DD-MM-YYYY)	2. REPORT TYPE	3. DATES COVERED (From - To)
	New Reprint	-

4. TITLE AND SUBTITLE
Application of a dynamic-mixture shock-wave model to the metal–matrix composite materials

5a. CONTRACT NUMBER
W911NF-09-1-0513

5b. GRANT NUMBER

5c. PROGRAM ELEMENT NUMBER
622105

6. AUTHORS
M. Grujicic, B. Pandurangan, W.C. Bell, C.-F. Yen, B.A. Cheeseman

5d. PROJECT NUMBER

5e. TASK NUMBER

5f. WORK UNIT NUMBER

7. PERFORMING ORGANIZATION NAMES AND ADDRESSES
Clemson University
Office of Sponsored Programs
300 Brackett Hall
Clemson, SC 29634 -5702

8. PERFORMING ORGANIZATION REPORT NUMBER

9. SPONSORING/MONITORING AGENCY NAME(S) AND ADDRESS(ES)
U.S. Army Research Office
P.O. Box 12211
Research Triangle Park, NC 27709-2211

10. SPONSOR/MONITOR'S ACRONYM(S)
ARO

11. SPONSOR/MONITOR'S REPORT NUMBER(S)
56526-EG.10

12. DISTRIBUTION AVAILIBILITY STATEMENT
Approved for public release; distribution is unlimited.

13. SUPPLEMENTARY NOTES
The views, opinions and/or findings contained in this report are those of the author(s) and should not contrued as an official Department of the Army position, policy or decision, unless so designated by other documentation.

14. ABSTRACT
The so-called “dynamic mixture” model is applied to a prototypical metal matrix composite (MMC) system (consisting of an aluminum matrix and SiC particulates) in order to investigate the propagation of planar (i.e. one directional), longitudinal (i.e. uniaxial strain), steady (i.e. time-invariant) structured shock waves. Waves of this type are typically generated during blast-wave loading or ballistic impact and play a major role in the way blast/ballistic impact loads are introduced into a structure. Hence, the knowledge of

15. SUBJECT TERMS
Structured shocks, Dynamic-mixture model, Metal–matrix composites

16. SECURITY CLASSIFICATION OF:			17. LIMITATION OF ABSTRACT	15. NUMBER OF PAGES	19a. NAME OF RESPONSIBLE PERSON
a. REPORT	b. ABSTRACT	c. THIS PAGE			Mica Grujicic
UU	UU	UU	UU		19b. TELEPHONE NUMBER: 864-656-5639

Report Title

Application of a dynamic-mixture shock-wave model to the metal–matrix composite materials

ABSTRACT

The so-called “dynamic mixture” model is applied to a prototypical metal matrix composite (MMC) system (consisting of an aluminum matrix and SiC particulates) in order to investigate the propagation of planar (i.e. one directional), longitudinal (i.e. uniaxial strain), steady (i.e. time-invariant) structured shock waves. Waves of this type are typically generated during blast-wave loading or ballistic impact and play a major role in the way blast/ballistic impact loads are introduced into a structure. Hence, the knowledge of their propagation behavior is critical for designing structures with superior blast and impact protection capacities.

To validate the computational procedure used, the structured shock-wave analysis is first applied to a homogeneous (i.e. single component) metallic system (commercially pure niobium). Next, the analysis is applied to the aforementioned MMC (in the limit of intermediate to strong shocks) when the contribution of the stress deviator to the total stress state can be neglected. Finally, the computational results are compared with their experimental counterparts available in the open literature in order to validate the dynamic-mixture method used.

REPORT DOCUMENTATION PAGE (SF298)
(Continuation Sheet)

Continuation for Block 13

ARO Report Number 56526.10-EG
Application of a dynamic-mixture shock-wave m ...

Block 13: Supplementary Note

Approved for public release; distribution is unlimited.

Materials Science and Engineering A 528 (2011) 8187–8197

Contents lists available at ScienceDirect

Materials Science and Engineering A

journal homepage: www.elsevier.com/locate/msea

Application of a dynamic-mixture shock-wave model to the metal–matrix composite materials

M. Grujicic[a,*], B. Pandurangan[a], W.C. Bell[a], C.-F. Yen[b], B.A. Cheeseman[b]

[a] Department of Mechanical Engineering, Clemson University, Clemson, SC 29634, United States
[b] Army Research Laboratory, Survivability Materials Branch, Aberdeen, Proving Ground, MD 21005-5069, United States

ARTICLE INFO

Article history:
Received 24 March 2011
Received in revised form 8 July 2011
Accepted 4 August 2011
Available online 11 August 2011

Keywords:
Structured shocks
Dynamic-mixture model
Metal–matrix composites

ABSTRACT

The so-called "*dynamic mixture*" model is applied to a prototypical metal matrix composite (MMC) system (consisting of an aluminum matrix and SiC particulates) in order to investigate the propagation of planar (i.e. one directional), longitudinal (i.e. uniaxial strain), steady (i.e. time-invariant) structured shock waves. Waves of this type are typically generated during blast-wave loading or ballistic impact and play a major role in the way blast/ballistic impact loads are introduced into a structure. Hence, the knowledge of their propagation behavior is critical for designing structures with superior blast and impact protection capacities.

To validate the computational procedure used, the structured shock-wave analysis is first applied to a homogeneous (i.e. single component) metallic system (commercially pure niobium). Next, the analysis is applied to the aforementioned MMC (in the limit of intermediate to strong shocks) when the contribution of the stress deviator to the total stress state can be neglected. Finally, the computational results are compared with their experimental counterparts available in the open literature in order to validate the dynamic-mixture method used.

1. Introduction

Metal–matrix composites (MMCs) are among the most advanced commercially available materials nowadays. These materials are seeing increased use in the following applications: automotive-engineering (e.g. crash-worthy structures), aerospace industry (e.g. space debris impact shields), and defense industry (e.g. light-weight, high-performance blast and ballistic protection systems) [1]. The main reason for the aforementioned increased application of this class of composite materials is their ability to simultaneously satisfy a variety of manufacturing/processing constraints and functional/performance requirements (via material property tailoring). Specifically, as implied by the aforementioned applications, this class of composites tends to provide good performance under high loading-rate conditions. Clearly, a further increase in the high loading-rate application of these materials necessitates enhanced knowledge of both the phenomena associated with shock-wave generation and propagation (addressed in the present work), as well as the micro-structure evolution and material deformation/degradation processes accompanying shock propagation (to be addressed in our future work).

When analyzing shock-wave generation and propagation within MMCs and the associated microstructure-evolution and material deformation/degradation processes, one must address a number of issues specific to this class of materials, among which the following play a prominent role:

(a) MMCs are heterogeneous (i.e. at least two phase) materials in which the constituent phases (a metallic matrix and, typically, ceramic reinforcements and potentially voids) generally possess very different microstructural, physical, mechanical, and morphological properties and volume fractions;
(b) MMCs may be elastically and/or inelastically anisotropic; and
(c) The effective properties of the MMCs are not often defined solely by a rule-of-mixture applied to the constituent material properties, but may also be greatly affected by the properties of the matrix/reinforcement interphase boundaries.

These three issues can give rise to a broad range of relations between propagating shock waves, initial material microstructure and the material structure resulting from the passage of shock waves. The increasing utilization of the MMCs in future, more-demanding engineering designs necessitates an improved knowledge of the basic phenomena associated with shock wave generation and propagation within the MMCs and the associated material microstructure/property changes. The focus of the present

* Corresponding author at: 241 Engineering Innovation Building, Clemson, SC 29634-0921, United States. Tel.: +1 864 656 5639; fax: +1 864 656 4435.
E-mail address: gmica@clemson.edu (M. Grujicic).

0921-5093/$ – see front matter © 2011 Elsevier B.V. All rights reserved.
doi:10.1016/j.msea.2011.08.008

work is on the phenomena related to the propagation of shock waves within the heterogeneous isotropic solids (like some classes of MMCs such as those based on particulate reinforcements).

The development of complex composite-material structures such as the ones mentioned above typically includes extensive experimental test programs. Such experimental test programs are critical for ensuring the utility and effectiveness of the composite-material structures. However, the use of experimental test programs is generally expensive, time-consuming and often involves destructive testing. While the role of experimental test programs remains critical, they are increasingly being complemented by the corresponding computation-based engineering analyses and simulations. The knowledge of composite-material response under various in-service loading conditions, as described by the corresponding material model(s), is one of the key components in such analyses greatly affecting their utility and fidelity. The main objective of the present paper is to help advance the use of these computational engineering analyses and simulations in the areas of design and application of the MMC structures by further developing the analysis and the knowledge of the phenomena associated with shock propagation in the MMCs.

An overview of the public-domain literature carried out as part of the present work revealed a number of material models for the MMCs. There are different ways in which these models can be classified. For example, MMC-material models can be classified according to the microstructure length scale which is being emphasized in the model. In accordance with this classification continuum [e.g. 2], grain-size [e.g. 3] and atomic-scale [e.g. 4] MMC-material models can be identified. Alternatively, MMC material models can be classified according to the morphology (and size) of the reinforcements as whiskers-reinforced MMCs [5], particulate-reinforced MMCs [6], dispersion-reinforced MMCs [7], etc.

The MMC-material model classification adopted in the present work is based on the applicability of the models with respect to the different loading-rate/deformation-rate ranges. In other words, the models identified in the open literature are divided into: (a) those suitable for quasi-static and/or sub-sonic dynamic deformation rate conditions [8]; and (b) those suitable for super-sonic (i.e. shock-wave) loading conditions [9]. While there are material models in the literature which retain the discrete nature of the two MMC-material components (i.e. of the metallic matrix and the discrete reinforcements), the ones considered in the present work treat the MMC as a homogenized/smeared out mixture of the two components. The main reason for this is that the interest of the present work was into MMC-material models which are suitable for large-scale computational investigations. In these investigations, due to a prohibitively high computational cost, one cannot afford to treat the MMC material as a heterogeneous two-component medium, but is forced to consider the same as a homogenized/smeared-out "*single-component*" material.

Various MMC-material models from the two aforementioned classes differ generally in the way the two components are mixed/homogenized. That is different assumptions are involved regarding partitioning of stresses and strains between the reinforcements and the matrix. In the majority of the material models, reviewed as part of the present work, the volume fraction of the MMC-material components is assumed to remain unchanged during loading/deformation. While this assumption can be generally justified in the case of quasi-static and sub-sonic dynamic loading conditions (which are associated with relatively small volumetric strains), its validity becomes questionable, as will be shown later, in the case of shock-wave loading (a type of loading which is dominated by the spherical/hydrodynamic component of the stress tensor and may result in large volumetric strains). In other words, as will be shown in next section, the volume fractions of the MMC components tend to behave as dynamic variables whose values depend on the current state of loading of the MMC at a given material point.

In the present work, an attempt is made to further advance and provide more physical insight into the so-called "*dynamic-mixture*" material model originally proposed by Drumheller [10] and Anderson et al. [11]. The model was aimed at capturing the effective response of MMCs when subjected to shock-wave loading. The model is of a homogenization-type, i.e. each material point is assumed to contain both of the MMC components. Also, while the mass fractions of the components remain constant at each material point, the corresponding volume fractions, as mentioned above, may evolve with dynamic loading. Consequently, one cannot derive a priori an effective material model by fixing volume fractions of the two constituents and combining their respective material models in accordance with some rule-of-mixture. Instead, the effective (loading-path dependent) volume fractions of the constituents at each material point have to be computed while solving the governing (mass, linear momentum and energy) conservation/balance equations.

When dealing with the mechanical-response of materials subjected to shock loading, among several others, the following two phenomena should be considered:

(a) shock waves are dominated by their longitudinal component, the component within which the material-particle propagation direction (as defined by the polarization vector) is collinear with the wave propagation direction (as defined by the wave vector). In other words, under shock-loading conditions, the stress state of the material is of (or nearly of) a uniaxial-strain (i.e. tri-axial stress) character. Furthermore, in the presence of shear-based inelastic/plastic deformation processes, and under sufficiently strong shock loading conditions, the stress state of the material is dominated by its hydrodynamic part, i.e. pressure. Consequently, it is often advantageous to treat the materials under investigation subjected to shock loading as being fluid-like (since stress state in fluids is pressure dominated); and
(b) under super-sonic strain rates associated with shock loading and due to the compliant/deformable nature of the metallic matrix, shock loading can be in general, associated with major internal thermal-energy/temperature increases. While long-range thermal-conduction effects are normally neglected (due to short-duration of the shock loading), one still has to address the problem of internal thermal-energy exchange/transfer between the MMC components residing at the same material point. This problem is typically handled by investigating MMC response under the adiabatic (no internal thermal-energy exchange, considered in the present work) and the isothermal (complete temperature equilibration) limits. It should be recognized, however, that under normal shock-loading conditions, each material-point may experience different extents of the internal thermal-energy exchange between its components.

In the present work, a critical examination of the "*dynamic-mixture*" material model [10,11] is first carried out. Next, the model is applied to aluminum-matrix MMCs reinforced with silicon carbide particulates. However, before applying the numerical procedure to the MMC material, the procedure was tested using a homogeneous isotropic material (commercially pure niobium).

The organization of the paper is as follows: the case of shock wave propagation within homogeneous isotropic solids including the definition of the governing equations and the material model as well as the presentation of the results of a structured shock-wave analysis is provided in Section 2. A critical review of the dynamic-mixture model and the application of this model to the aluminum matrix + silicon carbide reinforced MMC is provided in

Section 3. The key conclusions resulting from the present study are summarized in Section 4.

2. Structured shocks in isotropic homogeneous solids

2.1. Analysis

Before analyzing the mechanical response of composite materials to super-sonic dynamic (i.e. shockwave-based) loading, one should briefly overview the corresponding problem in the single-component material case. First, it should be recognized that in single-component materials, shock waves propagate not as discontinuities in the material state variables (e.g. stress, strain, density, temperature, etc.), but rather as (smooth) structured waves (i.e. the material state variables vary smoothly across the shock-wave front, although the wave-front thickness may be quite small). The thickness of the shock-wave front is controlled by the competition between two aspects of the material mechanical response: (a) nonlinear material constitutive response which gives rise to an increase in the material stiffness with an increase in the deformation. This phenomenon leads to steepening of the wave front (i.e. to a reduced shock wave front thickness) as the trailing high-stress/pressure portions of the wave tend to propagate at a higher speed than their leading low-stress/pressure counterparts; and (b) rate-dependent material constitutive response which gives rise to an increase in the energy dissipation with an increase in the loading rate. This, in turn, causes a deceleration in the fast-propagating high-stress/pressure portions of the wave and produces a wave-dispersion effect. The final profile acquired by the shock wave is the result of the balance between the nonlinear-constitutive response induced steepening effects and the rate-dependency induced dispersion effects.

Shock-wave propagation-induced deformation processes are controlled by the mass, momentum and energy conservation laws which can be defined within a three-dimensional Eulerian (spatial) framework as:

Conservation of mass: (provides a relationship between the motion of the material particles and the mass density)

$$\dot{\rho} + \rho \frac{\partial \dot{x}_\alpha}{\partial x_\alpha} = 0 \tag{1}$$

Conservation of momentum: (provides a relationship between the motion of the material particles and the equilibrium and the dissipative stresses/pressures)

$$\rho \ddot{x}_\alpha = -\frac{\partial}{\partial x_\alpha}(P+Q) + \rho f_\alpha + \frac{\partial S_{\alpha\beta}}{\partial x_\beta} \tag{2}$$

Conservation of energy: (provides a relationship between the mechanical work done and the stored strain and thermal energies)

$$\rho \dot{E} = (P+Q)\frac{\dot{\rho}}{\rho} + S_{\alpha\beta}\dot{\varepsilon}_{\alpha\beta} + \rho r \tag{3}$$

where ρ is the material mass-density, f is the mass-based body-force, x_α the α-th spatial coordinate, $\dot{x}_\alpha$ α-th component of the particle velocity (defined as a time derivative of the particle spatial coordinates), $S_{\alpha\beta}$ are the components of the stress deviator, $\dot{\varepsilon}_{\alpha\beta}$ are the corresponding strain-rate components and r is the external heat supply. The summation convention is implied by the repeated subscripts α, $\beta = 1, 2, 3$. The raised dot denotes a material derivative ($= \partial/\partial t + \partial/\partial x_\alpha \dot{x}_\alpha$). P is the (equilibrium/physical) pressure, Q is the dissipative-pressure, and E is the mass-based internal-energy density.

In a three-dimensional case as defined above, Eqs. (1)–(3) constitute a set of five equations with twelve unknowns: ρ, v_α ($\alpha = 1, 2, 3$), E, P, Q and $S_{\alpha\beta}(\alpha, \beta = 1, 2, 3)$, $S_{\alpha\beta} = S_{\beta\alpha}$, $S_{\alpha\alpha} = 0$. It should be noted that $\dot{\varepsilon}_{\alpha\beta}(\alpha, \beta = 1, 2, 3)$ is not considered as a separate dependent variable since $\dot{\varepsilon}_{\alpha\beta} = \partial v_\alpha / \partial x_\beta$. The independent variables in the problem at hand are the spatial coordinates $x_\alpha(\alpha = 1, 2, 3)$ and time, t.

To remove the under-determinacy of the above system of equations seven additional relations need to be defined. These include:

(a) One equation of state (EOS), $P = func(\rho, E)$;
(b) Five strength-model equations, $S_{\alpha\beta} = func(\varepsilon_{\gamma\delta})$, where $\alpha, \beta, \gamma, \delta = 1, 2, 3$; and
(c) One constitutive relation for the dissipative-pressure/artificial-viscosity $Q = func(\rho, \dot{\rho}, E)$;

It should be noted that, while the EOS and the strength-model are expected to account for the essential physics of high-strain-rate deformation of the material in question, the (artificial-viscosity based) Q term is often non-physical and is mainly used to help deal with the numerical/computational difficulties (i.e. to overcome the problems associated with numerical oscillations at the shock-wave front). The use of this term within a finite difference/element computational framework has been shown to help smear out the shock-wave front over several computational cells/elements. Consequently, the $Q = func(\rho, \dot{\rho}, E)$ relation is constructed in such a way that Q takes on significant (non-zero) values only in the shock-wave front region and $Q \to 0$ as $\dot{\rho} \to 0$ (in the regions away from the shock-wave front). It should be also noted that in the cases of rate-dependent materials, the use of the artificial-viscosity based Q term is often not necessary since the material, by itself, dissipates energy and assists in the formation of oscillation-free structured shocks.

The set of equations given above (plus the missing material specific equations) defines a general three-dimensional wave propagation problem. However, in this section, only the problem of propagation of steady (i.e. time invariant), plane (i.e. one-dimensional), longitudinal (i.e. uniaxial motion) shock-waves within isotropic homogeneous materials is considered. In this case, a single stationary shock-wave approach (i.e. attaching the reference frame to the moving shock-wave front) will be used. Consequently, it will be more convenient to deal with the one-dimensional mass, momentum and energy conservation equations within a (material) Lagrangian framework. In addition, the stress-deviator dependent term will be combined with pressure to obtain the axial stress, t_{11}, and the Q-dependent terms will be omitted (since the material constitutive equation will include a viscous term, also, the body force term in Eq. (2) and the external heat supply term in Eq. (3) will not be considered).

2.2. Numerical example

As established by Davison [12], the speed of propagation of a structured shock, C, is the same as the Lagrangian shock speed, U_s, for a discontinuous shock of the same amplitude (i.e. for the same change in the material states from those in front of the shock, referred to as "*minus*" state variables, to those behind the shock, referred to as the "*plus*" state variables). In addition, the shock jump conditions for the state variables must be satisfied between all pairs of points in a structured shock.

By combining the Lagrangian forms of the mass and momentum jump conditions:

$$\rho_R \;\; U_s \langle -v \rangle = \langle \dot{x} \rangle \tag{4}$$

$$\rho_R \;\; U_s \langle \dot{x} \rangle = \langle -t_{11} \rangle \tag{5}$$

where $\langle\,\rangle$ denote jumps in the quantities across the shock, the following relation is derived between the jumps in the stress and specific volume for a structured shock:

$$-t_{11}(Z) + \rho_R \;\; U_S^2 \left[\frac{v(Z)}{v_R} - 1 \right] = 0 \tag{6}$$

where the spatial coordinate Z, is defined as $Z = X - U_s \cdot t$ and, for simplicity, the attention is restricted to the following minus states case: $t_{11}^{-} = 0$ and $v^{-} = v_R$.

The materials analyzed in this section are assumed to be non-linear elastic (specifically described through the use of third order elastic constants) and linearly viscous. The stress relation for this material can be written as:

$$t_{11} = t_{11}^{E} + t_{11}^{V} \tag{7}$$

where

$$t_{11}^{E} = \frac{1}{2}\frac{v}{v_R}\left[\left(\frac{v}{v_R}\right)^2 - 1\right]\left\{\lambda + 2\mu + \frac{1}{4}(v_1 + 6v_2 + 8v_3)\left[\left(\frac{v}{v_R}\right)^2 - 1\right]\right\} \tag{8}$$

represents the elastic response with λ and μ being the linear (second order) Lamé elastic constants and v_1, v_2 and v_3 are the non-linear (third-order) elastic constants [12]. It should be noted that $((1/2)(v/v_R))[(v/v_R)^2 - 1]$ represents the 11-component of the large-deformation strain which is defined as a product of the 11-component of the deformation gradient and the 11-component of the Green Lagrangian strain.

The linear viscous contribution to the stress is given by

$$t_{11}^{V} = \omega d_{11} = \omega\frac{\dot{v}}{v} \tag{9}$$

where $\omega > 0$ is a viscosity coefficient.

In a structured steady shock, the following relation holds:

$$\dot{v} = \frac{dv}{dZ}\frac{dZ}{dt} = \frac{dv}{dZ}(-U_S) \tag{10}$$

Then, substitution of Eq. (10) into Eq. (9) yields:

$$t_{11}^{V} = -\frac{\omega U_S}{v}\frac{dv}{dZ} \tag{11}$$

Substitution of Eqs. (11) and (8) into Eq. (7) and that result into Eq. (6) yields:

$$\frac{d(v/v_R)}{dZ} = \frac{v/v_R}{\omega U_S}\left[t_{11}^{E} - \rho_R U_S^2\left(\frac{v}{v_R} - 1\right)\right] \tag{12}$$

Integration of Eq. (12), gives the structured shock waveform for the specific volume, $v(Z)$.

The corresponding stress waveform ($t_{11}(Z)$) can then be obtained from Eq. (6). The Lagrangian shock speed, U_s, appearing in this equation is obtained as follows: the shock strength/amplitude is first defined by specifying the magnitude of v^{+}. Then Eq. (8) is used to compute t_{11}^{E} while t_{11}^{V} is set to zero since $\dot{v}$ is essentially zero at distances far-away from the shock front. Then, by combining Eqs. (6)–(8), one can determine U_s.

The corresponding particle velocity waveform ($\dot{x}$ (Z)) can next be obtained from Eq. (1). Finally, the internal energy structured-shock waveform can be obtained from the Lagrangian form of the energy balance equation defined as:

$$E(Z) = \frac{1}{2}\dot{x}(Z)^2 \tag{13}$$

The specific example analyzed in the present section involves commercially pure niobium. The general and mechanical properties of this material are defined as: reference density, $\rho_R = 8700\ \mathrm{kg/m^3}$; Young's modulus, $E^* = 110$ GPa; Poisson's Ratio, $\nu = 0.4$; Lame' constants: $\lambda = (E^*\nu)/(1+\nu)(1-2\nu) = 157$ GPa and $\mu = E^*/2(1+\nu) = 39$ GPa [12]; the third order elastic constants, $v_1 = -301$ GPa; $v_2 = -131$ GPa and $v_3 = -104$ GPa [13]; the yield stress $\sigma_y = 350$ MPa (as cold-worked condition) and viscosity $\omega = 1.0$ Pa s [14]. The Hugoniot Elastic Limit (HEL) i.e. the axial stress at the onset of plastic yielding $t_{11}^{HEL} = ((\lambda + 2\mu)/2\mu)\sigma_y = 1.09$ GPa.

Examples of the results obtained in this portion of the work are given in Figs. 1–3.

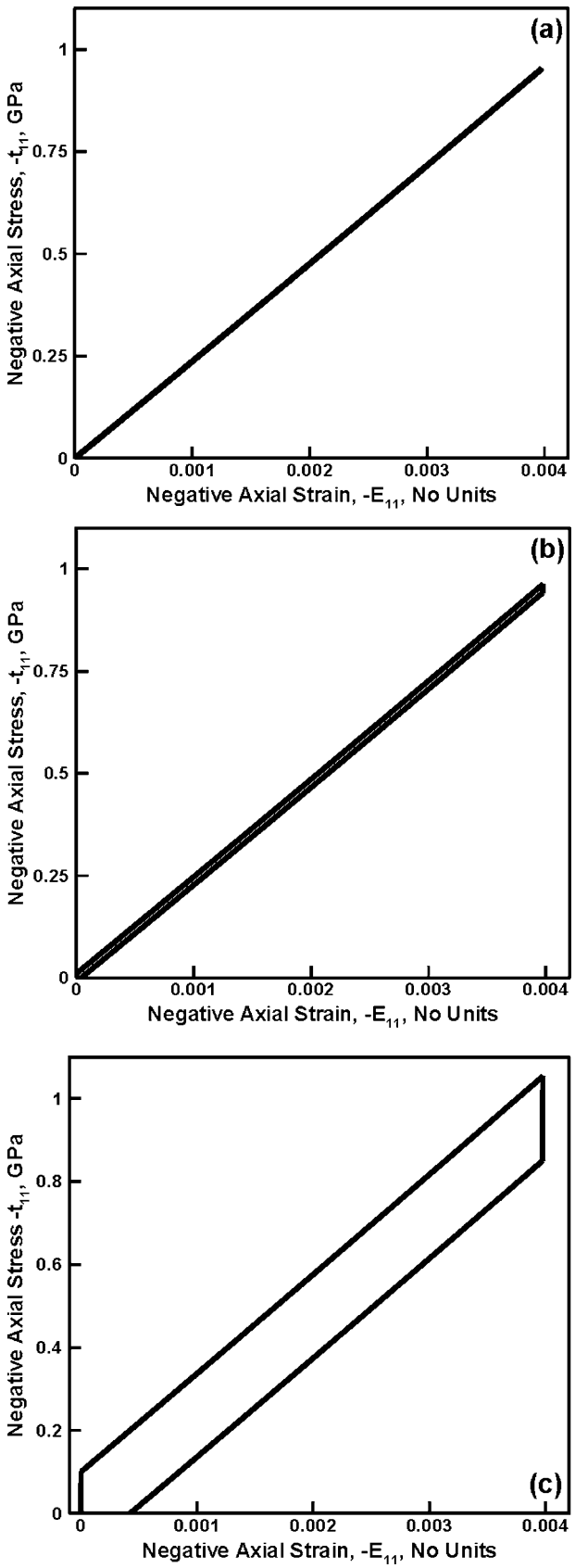

Fig. 1. Negative axial stress vs. negative axial strain for commercially pure niobium at strain rates of (a) $10^5\ s^{-1}$; (b) $10^6\ s^{-1}$; and (c) $10^7\ s^{-1}$.

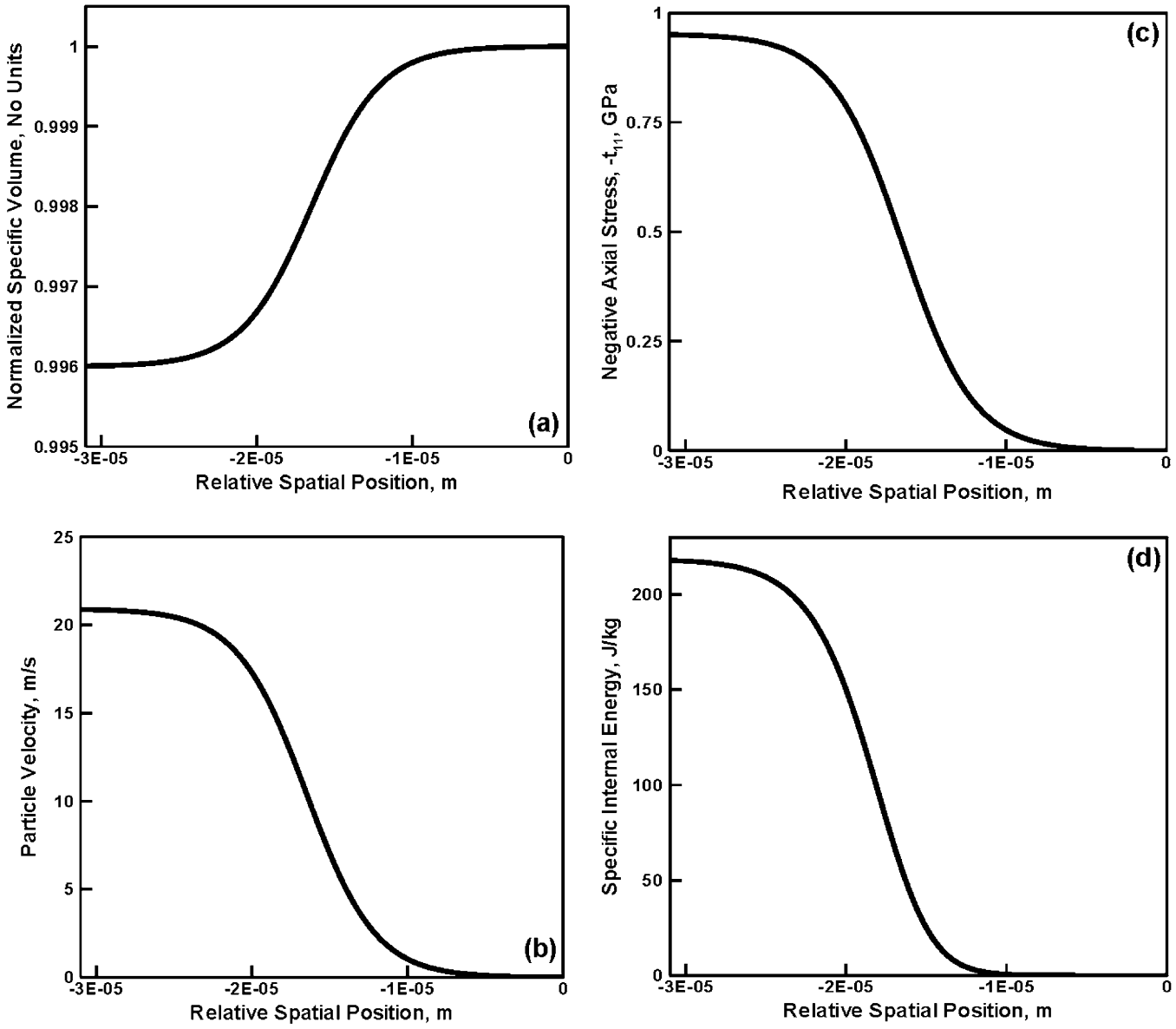

Fig. 2. Spatial structured-shock waveforms for (a) specific-volume normalized by reference specific volume; (b) particle velocity; (c) negative axial stress; and (d) mass-based internal energy density for commercially pure niobium shock loaded to near its Hugoniot Elastic Limit (HEL).

In Fig. 1(a)–(c), the effect of constant strain-rate on the $-t_{11}$ vs. $-E_{11}$ curve is depicted. It is clear that as the rate of loading increases, the extent of energy dissipation (as quantified by the area surrounded by the loading and the unloading parts of the $-t_{11}$ vs. $-E_{11}$ curve) increases. It should be also noted that the shock strength was kept relatively small in order to avoid the onset of plastic deformation. Plastic deformation gives rise to a second (trailing) shock wave and the associated two-shock analysis is beyond the scope of the present work.

Fig. 2(a)–(d) show respectively the specific volume, (negative) axial stress, particle velocity and internal energy density structured shock wave fronts, respectively. It should be noted that: (a) no artificial viscosity was used in these calculations since the material, through its own rate-dependent viscous behavior gives rise to the formation of a structured shock; and (b) the presence of a viscous term affects the shape of the shock front converting it from a discontinuity to a smooth transition, but does not affect the magnitude of the plus-state variables. It should be further noted that the results displayed in Fig. 2(a)–(d) pertain to the spatial shock-wave profiles (the ones which would be recorded by a camera attached to the propagating shock). To obtain the corresponding temporal shock wave-forms (the one which would be recorded by a sensor located at a fixed material point), the horizontal axis in Fig. 2(a)–(d) should be divided by $-U_s$.

Fig. 3(a)–(b) show respectively the variations of the (negative) axial stress and the particle velocity with the material specific volume. It is seen that the variations are of a linear-type confirming that the material evolution accompanying the passage of a structured shock takes place along the respective "*Rayleigh*" line. This type of material evolution is the reason that, as mentioned earlier, the shock-jump relations must hold between any two points of the shock wave-form.

It should be noted that, within the present formulation commercially pure niobium is treated as a homogeneous isotropic material. This is an approximation since this material is of a polycrystalline nature, i.e. it is composed of a large number of grains/crystallites (and also contains a variety of surface, line and point defects). Hence, the present formulation is more appropriate in the weak-shock limit in which the shock wave front thickness is relatively large in comparison to the average grain size of the

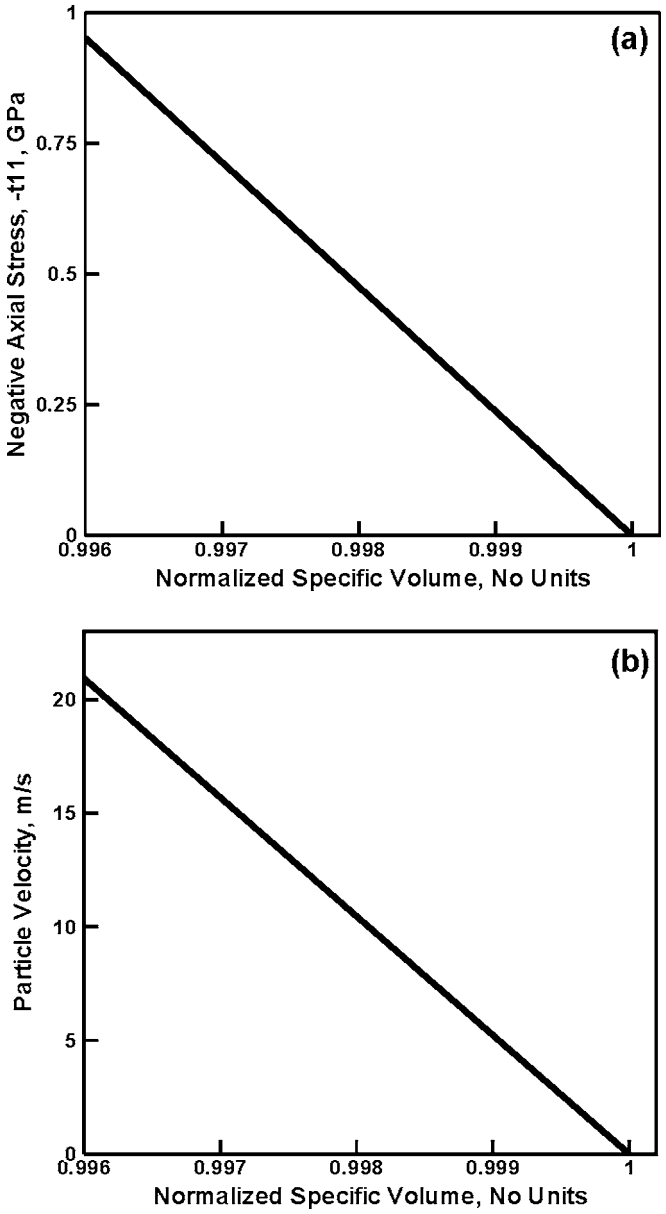

Fig. 3. Inter-relationships between (a) axial stress and specific volume; and (b) particle velocity and specific volume across the structured-shock wave front in commercially pure niobium impulsively loaded to near its HEL state.

material. This is the limit examined in the present section. As correctly pointed out by one of the reviewers of the present work, within a more rigorous framework, commercially pure niobium would have to be treated as a heterogeneous material so that the interaction of the shock-wave with individual grains and grain boundaries is accounted for. This type of shock-physics framework has been developed over the last several years e.g. [18,19]. Within these newer formulations, the effect of material microstructure is brought in using the theory of crystal plasticity which recognizes unique orientation of the local crystallite. Application of these new formulations to planar shocks revealed that the as-shocked material-state fields are greatly affected by the thickness of the shock-wave front, i.e. by the shock strength. That is, in the strong-shock regime, as-shocked material state is highly heterogeneous at a super grain-size length scale and fairly homogeneous within individual grains. In sharp contrast, in the weak-shock regime, the as-shocked material state tends to be more uniform and approaches the one obtained in the present work.

3. Structured shocks in isotropic heterogeneous solids

3.1. Analysis

In this section, a brief critical overview is provided of the dynamic-mixture composite-material model originally developed by Drumheller [10] and Anderson et al. [11]. As mentioned earlier, this is an example of a homogenization composite-material model, within which each material point is assumed to contain all the constituent phases (components) of the material. However, component mixing is carried out dynamically (i.e. the component volume fractions are not considered as constant but rather treated as dynamic, solution-dependent variables). It should be also noted that the analysis presented below is limited to shocks of at least intermediate strength so that the contribution of the stress deviator to the total stress can be neglected and, hence, the stress-state can be assumed to be of a spherical (hydrodynamic) character. Furthermore, the analysis is restricted to two component heterogeneous solids (although it can be readily extended to multi-component systems).

To explain the foundation of the dynamic mixture theory [10], separate consideration will be given to the three conservation/balance equations, Eqs. (1)–(3).

Mass conservation equation: The first key assumption in the dynamic-mixture model is based on the recognition that within the extremely short time associated with shock-wave loading, relative motions between the components within a single material point can be neglected (i.e. particle velocities for the components associated with the same material point are assumed to be equal). Consequently, Eq. (1) can be applied to the homogenized/smeared-out material. However, as will be explained below one must at this point recognize the two-component character of the composite material and introduce additional state variables such as

(a) intrinsic mass density of each component, $\bar{\rho}_\varepsilon$, $\varepsilon = 1, 2$;
(b) volume fraction of each component, ϕ_ε, $\varepsilon = 1, 2$;
(c) partial density of each component, ρ_ε, $\varepsilon = 1, 2$; and
(d) (constant) mass fraction of each component, M_ε, $\varepsilon = 1, 2$.

These state variables are not all independent but rather are related through the following set of equations:

$$\sum_\varepsilon \phi_\varepsilon = 1 \tag{14}$$

$$\rho_\varepsilon = \phi_\varepsilon \bar{\rho}_\varepsilon \tag{15}$$

$$\rho = \sum_\varepsilon \rho_\varepsilon \tag{16}$$

$$M_\varepsilon = \frac{\rho_\varepsilon}{\rho} \tag{17}$$

Combining Eqs. (15) and (17) yields:

$$\bar{\rho}_1 = \frac{M_1 \rho}{\phi_1} \tag{18}$$

$$\bar{\rho}_2 = \frac{M_2 \rho}{\phi_2} \tag{19}$$

Momentum conservation equation: The second key assumption in the dynamic-mixture model is the equality of total pressure ($P+Q$) between the two constituents within each material-point/computational-cell. This equality can be stated as:

$$P_1 + Q_1 = P_2 + Q_2 = P + Q \tag{20}$$

where the quantities with subscripts pertain to the individual components while the quantities without subscripts pertain to

the homogenized/smeared-out material. One can next show that the pressure-equality assumption defined by Eq. (20) makes the component volume fractions ϕ_ε non-constant. To prove this, the following simple thought experiment can be carried out. Consider a single cube-shaped computational-cell which contains the two components at equal (0.5) volume fractions. Next, assume that each of the two components resides in single computational sub cells with the inter-component boundary being parallel with one of the faces of the cube. The cell is next subjected to uniaxial-strain loading in a direction parallel with the inter-component boundary. To satisfy the equal-pressure condition, the stiffer component must undergo a smaller volume change than the more compliant one. However, since both components are subjected to the same uniaxial-strain, this could be accomplished only if the components experience also a normal strain in a direction normal to the inter-component boundary. The latter strain would then give rise to a change in the volume fractions of the components. It should be noted that while the volume fractions of the two components may change under dynamic loading, the corresponding mass-fractions remain unchanged.

Due to the pressure equality defined by Eq. (20), one can use the original form of the momentum conservation equation, Eq. (2), for the homogenized/smeared-out material in which the sum of the equilibrium pressure P and the dissipative pressure Q is replaced with the corresponding sum for one of the components. The latter sum (as well as its counterpart for the other component) is defined by the use of an equation of state (EOS):

$$P_\varepsilon = \hat{P}_\varepsilon(\bar{\rho}_\varepsilon, E_\varepsilon) \tag{21}$$

and the (possibly artificial) energy-dissipation relation:

$$Q_\varepsilon = \hat{Q}_\varepsilon(\bar{\rho}_\varepsilon, \dot{\bar{\rho}}_\varepsilon, E_\varepsilon) \tag{22}$$

It should be noted that if the sum $P_\varepsilon + Q_\varepsilon$ is used in the momentum conservation equation then the dependent variables E for the homogenized material is replaced with a pair of variables ϕ_ε, E_ε.

Energy conservation equation: The third key assumption in the dynamic-mixture model is related to a total absence of the thermal-energy exchange between the two components located at the same material point. This adiabatic approximation is justified considering the microsecond nature of the shock-wave time scale. Due to the total absence of energy exchange between the components residing in the same computational cell (as well as between different cells), one has to define two energy conservation equations, one for each of the components as

$$\bar{\rho}_1\dot{E}_1 = (P_1 + Q_1)\frac{\dot{\bar{\rho}}_1}{\bar{\rho}_1} \tag{23}$$

$$\bar{\rho}_2\dot{E}_2 = (P_2 + Q_2)\frac{\dot{\bar{\rho}}_2}{\bar{\rho}_2} \tag{24}$$

Then the mass-based homogenized-material energy density is defined as:

$$E = \sum_\varepsilon M_\varepsilon E_\varepsilon \tag{25}$$

The System of Governing Equations:

The dynamic-mixture theory is next analyzed within a one-dimensional steady-wave propagation framework within which only motion along the x_1 direction is considered and all the state variables are taken to be functions of a single variable, $Z = x_1 - ut$, where u is the (Eulerian) speed of propagation of the steady wave. Since the x and t partial derivatives can be expressed in terms of a single total Z derivative, Eqs. (1)–(3) can be integrated in the limits of '*minus*' and '*plus*' states (where the Q term or terms can be neglected) to yield:

$$\frac{\dot{x}}{u} = 1 - \frac{\rho_0}{\rho} \tag{26}$$

$$P + Q = \rho_0 u\dot{x} \tag{27}$$

$$E = \frac{1}{2}\dot{x}^2 \tag{28}$$

Note that the Q-term is kept in Eq. (27) in order to imply that these equations hold anywhere along the shock waveform (including the regions where Q cannot be neglected).

Based on the analysis presented in this section thus far, one can establish that the dynamic-mixture model within the one-dimensional steady framework is defined by the following set of nine equations:

(a) one mass conservation equation, Eq. (26);
(b) one momentum conservation equation, Eq. (27);
(c) one energy conservation equations, Eq. (28);
(d) two pressure equality relations, Eq. (20);
(e) two EOS relations, Eq. (21); and
(f) two dissipation energy relations, Eq. (22).

The corresponding nine dependent state variables include: ϕ_1, ρ, $\dot{x}$, E_1, E_2, P_1, P_2, Q_1 and Q_2 where it is assumed that the shock strength is defined by the prescribed shock speed, u. Thus, the system of governing equations is determinate and can be solved (using a numerical scheme).

In Refs. [10,11], the dynamic mixture model was implemented into different wave-propagation computer programs and no detail regarding the solution of the governing equations was provided. In this work, the governing equations of the dynamic mixture model are critically evaluated (this was done in the preceding sections) and a detailed explanation of the numerical procedure is provided. First, functional forms of the EOSs and dissipative pressures relevant to the present work are reviewed in Appendices A and B, respectively. This is followed by Appendix C which outlines the procedure used to obtain the temperature Hugoniot. Finally, the numerical procedure developed to solve the governing dynamic-mixture model equations is presented in Appendix D.

3.2. Numerical example

The dynamic-mixture model overviewed in the previous section is applied in this section to a prototypical MMC (an aluminum matrix composite reinforced with micron-size SiC particulates). The MMC in question is typically fabricated using a pressure-less infiltration process [15] and, hence, is not expected to contain significant extents of elastic or plastic anisotropies. Consequently, the material will be treated as being isotropic and, due to a small-size of the particulates, the homogenization assumption utilized within the dynamic-mixture method appears justified. Also, the analysis is carried out in an intermediate- to high strength shock regime so that the material response can be taken to be dominated by its hydro-dynamic (e.g. pressure, density, etc.) quantities. Due to the use of the hydrodynamic approximation, the mechanical responses of the materials in question (i.e. the components of the MMC) are fully defined by the appropriate equation of state (EOS), a relationship between pressure, mass-density and mass-based internal energy density. More details of the EOS relations used can be found in Appendix A while the relevant material parameters are summarized in Table 1.

In addition to the EOS relations, the corresponding relations for the dissipative-pressure, Q, have to be defined. More details

Table 1
A summary of the material parameters for aluminum, SiC reinforcements and Al + SiC MMC. See Appendix A for details.

Parameter	Units	Aluminum	SiC	MMC
ρ_R	kg/m^3	2785	3215	2805
Γ_R	–	2.0	1.56	1.89
C_0	m/s	5328	N/A	N/A
S	–	1.338	N/A	N/A
A_1	GPa	N/A	220	88
A_2	GPa	N/A	361	171
A_3	GPa	N/A	0	120

of the functional forms used in the present work can be found in Appendix B.

The application of the numerical procedure mentioned in the previous section resulted in the structured-shock wave forms similar to those obtained for the homogeneous-material case, Fig. 2(a)–(d). These results are not included for brevity. Instead, the attention is focused on the Hugoniot relations, i.e. the relations which show the dependence of the plus-state quantities and the shock speed on the shock strength. An example of the results obtained in this portion of the work is displayed in Figs. 4–6.

In Fig. 4, a relationship is displayed between the (plus-state) pressure and the (plus-state) specific volume normalized by the reference specific volume. Low-pressure portion of this curve is shown using a dashed line in order to indicate that in this regime the hydrodynamic assumption is not valid (i.e. material strength effects cannot be neglected) and, hence, the predicted Hugoniot relations may not be valid. To establish the validity of the dynamic-mixture model used, pressure vs. normalized specific volume results obtained using an experimentally based EOS [16] are also displayed in Fig 4. The flyer-plate experimental results used in the construction of the puff-type experimentally-based EOS (Appendix A and Table 1) [16] are of a proprietary nature and could not be reported in the present manuscript. Examination of Fig. 4 reveals that the agreement between the computational results obtained in the present work and the "*experimental*" results is reasonable. It should be recalled that within the present dynamic-mixture formulation, pressure equality is postulated between the two phases

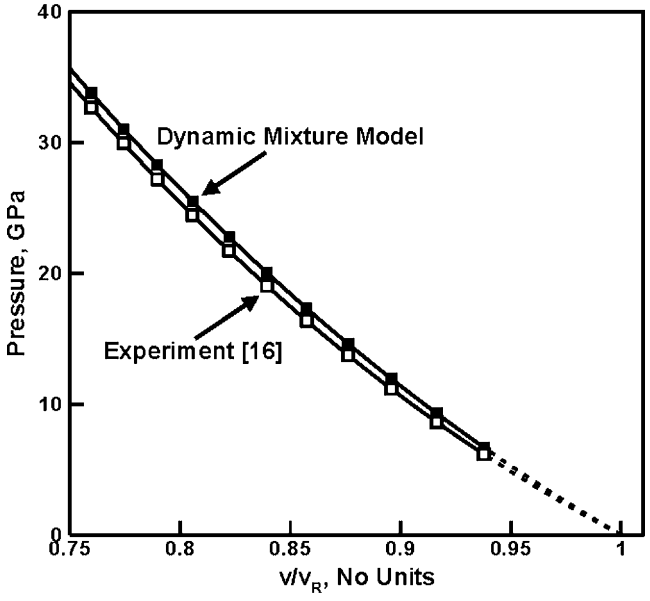

Fig. 4. Pressure vs. specific volume normalized by reference specific volume Hugoniot curve for the Al + SiC particulate (20 vol.%) metal–matrix composite. An experimentally derived corresponding curve for the same material is also depicted for comparison.

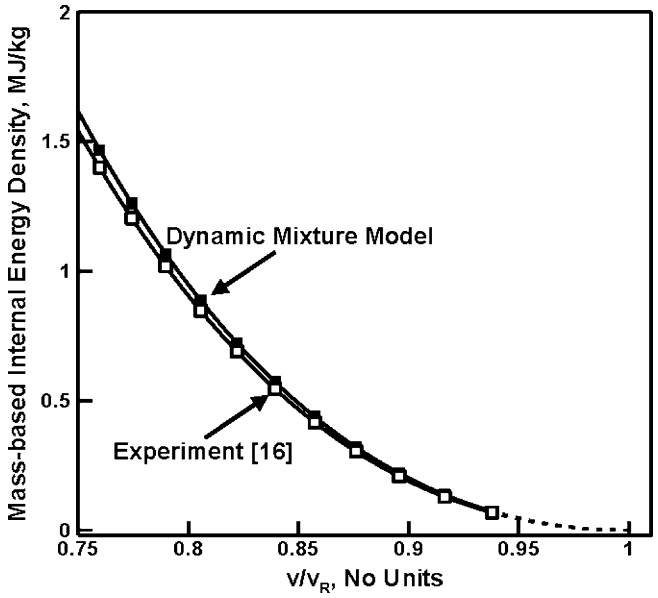

Fig. 5. Mass-based internal energy density vs. specific volume normalized by reference specific volume Hugoniot curve for the Al + SiC particulate (20 vol.%) metal–matrix composite. An experimentally derived corresponding curve for the same material is also depicted for comparison.

associated with the same material point. As correctly pointed out by one of the reviewers of the present manuscript, the pressure equality assumption leads to a lower bound of the composite material effective stress/pressure response. Thus, under other assumptions regarding the partitioning of pressure and deformation between the constituent phases one may expect somewhat lower degree of experiment/computation agreement than the one seen in Fig. 4.

The corresponding mass-based internal energy-density vs. specific volume normalized by the reference specific volume plot is displayed in Fig. 5. Again its counterpart based on the experimentally based Puff EOS is displayed for comparison. The agreement between the two sets of data is quite good.

The relationship between the shock-speed and particle velocity predicted by the current dynamic-mixture based calculations

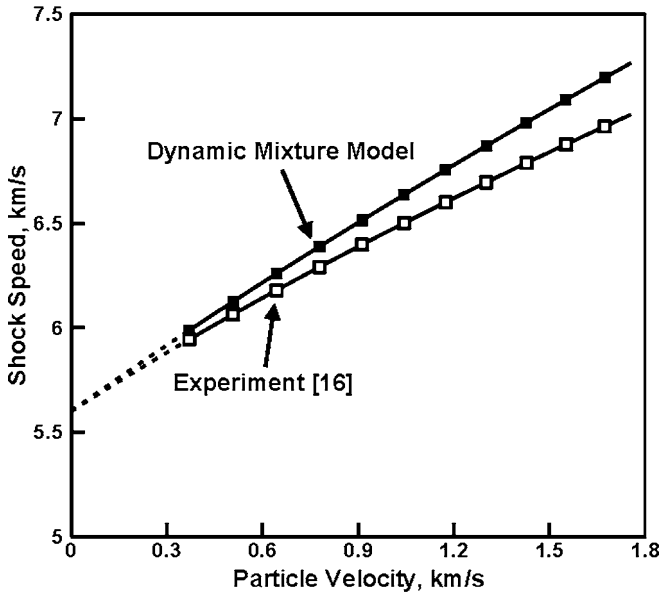

Fig. 6. Particle-velocity dependence of the shock speed for the Al + SiC particulate (20 vol.%) metal–matrix composite. An experimentally derived corresponding curve for the same material is also depicted for comparison.

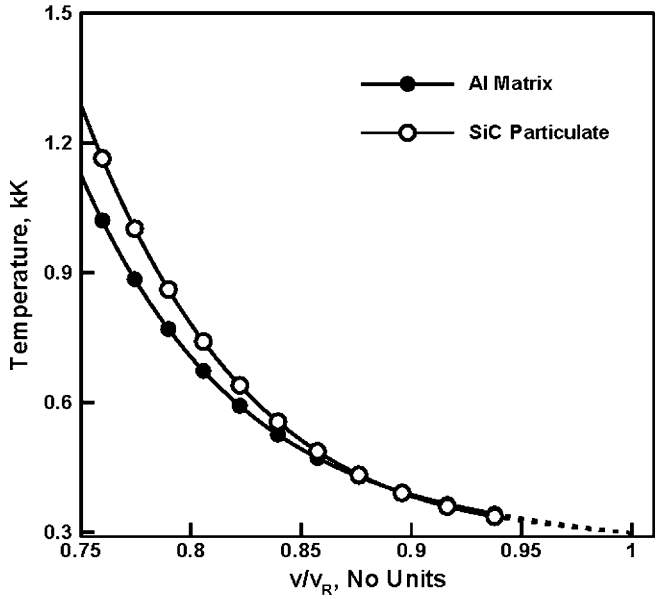

Fig. 7. MMC-component (i.e. Al-matrix and SiC particulate reinforcement) temperature vs. MMC specific volume normalized by reference specific volume Hugoniot curves for the Al + SiC particulate (20 vol.%) metal–matrix composite. Only the contributions of the irreversible character of shock loading are taken into account in the temperature calculations.

and the experimentally based EOS [16] are shown in Fig. 6. As mentioned earlier, the flyer-plate experimental results used in the construction of the experimentally based EOS [16] are of a proprietary nature and could not be reported in the present manuscript. Again, the agreement between the two sets of results is quite good and, in addition, suggests that the shock-speed vs. particle velocity relation is nearly a linear function, $U = C_0 + s\dot{x}$ with C_0 and s determined using a curve fitting procedure as: $C_0 = 5600$ m/s and $s = 0.78$.

The results displayed in Figs. 4–6 show that the three dynamic-mixture model based Hugoniot relations are in good agreement with their experimental counterparts. Since these cross-plot relations are essentially the projections of a Hugoniot curve defined within a multi-dimensional $P - v - E - \dot{x} - U_s$ space, onto a given two dimensional sub-space (e.g. P *vs.* v/v_R), one can conclude that the present dynamic-mixture based analysis fairly realistically accounts for the observed high-rate response of the MMC in question.

The last point addressed in the present work deals with the issue of temperature increase during shock-wave loading of the MMCs. There are two main mechanisms of energy dissipation within these materials during dynamic loading:

(a) Shock-loading along the Rayleigh line is a thermodynamically irreversible process and, in accordance with the second law of thermodynamics, is associated with an entropy increase i.e. internal energy dissipation; and
(b) The rate-dependent viscous portion of the material mechanical response gives rise to a dissipative pressure Q and the work done by this pressure during shock loading is (not stored as strain energy but rather) dissipated into heat, raising the material temperature.

To calculate the temperature increase due to thermodynamically irreversible character of shock loading, the procedure described in Appendix C was used. This procedure combines the Rankine–Hugoniot jump relation with an equation combining the first and the second laws of thermodynamics and takes advantage of a number of Maxwell-relations.

In Fig. 7, the Hugoniot plots pertaining to the temperatures of the two MMC components vs. the MMC specific volume normalized by the reference specific volume is displayed. In these calculations, the specific heats for the Al and SiC were assigned the values 870 J/kg K and 800 J/kg K, respectively [17]. The temperature data displayed were obtained by including only the contribution of the irreversible-thermodynamic nature of shock loading. While there are no experimental data that could be used for comparison, the results displayed in Fig. 7 clearly show that the resulting temperatures are so high that the MMC components will be (thermally) annihilated.

To obtain the corresponding temperature vs. specific volume normalized by the reference specific volume plots for the case when viscous dissipation is solely responsible for the energy dissipation, a procedure was devised which integrates the contribution of energy dissipation to the temperature increase (along the shock wave front). Since these results are highly sensitive to the details of the (not well known) Q relations for the two components of the MMC material, and due to the fact that the results displayed in Fig. 7already showed a complete MMC-material annihilation, the results obtained using this procedure are not presented.

4. Summary and conclusions

Based on the results obtained in the present work, the following summary remarks and main conclusions can be drawn:

1. The so-called "*dynamic-mixture*" model which postulates the absence of relative motion between the constituents of a mixture (a metal–matrix composite, in the present work), the absence of thermal-energy exchange and total-pressure equality is critically reviewed.
2. A numerical procedure is next developed to solve the governing differential, constitutive and constraining relations. The procedure is next validated using a single-component material (commercially pure niobium).
3. The procedure is next applied to a common aluminum-matrix SiC-particulate reinforced composites. In the limit of high loads (the hydrodynamic limit), this procedure yielded a number of Hugoniot relations which agreed reasonably well with their experimental counterparts.
4. Finally, sources (i.e. thermodynamic irreversibility and viscous dissipation) of the thermal effects associated with strong shock loading of the MMC in question are analyzed. The results obtained showed that the associated temperature increase is large enough to cause complete annihilation of the MMC in question.
5. It is planned to extend the dynamic-mixture model to the weak-shock regime in which the contributions of the stress deviator and plastic deformation to the material response need to be considered. In addition, the dynamic mixture model will be implemented into a user material subroutine so that general three-dimensional transient non-linear dynamics problems can be analyzed.

Acknowledgements

The material presented in this paper is based on work supported by the Army Research Office (ARO) research contract entitled "*Multi-length Scale Material Model Development for Armor-grade Composites*", Contract Number W911NF-09-1-0513, and the Army Research Laboratory (ARL) research contract entitled "*Computational Analysis and Modeling of Various Phenomena Accompanying*

Detonation Explosives Shallow-Buried in Soil" Contract Number W911NF-06-2-0042.

Appendix A. Equation of state (EOS)

As mentioned in the main body of the manuscript, EOS defines pressure dependence on density (i.e. degree of compression) and mass-based internal-energy density. In the present work, three forms of the EOS are used:

(a) the so-called "*shock*" EOS for the aluminum matrix [16];
(b) the so-called "*polynomial*" EOS for the silicon carbide reinforcements [16]; and
(c) the so-called "*puff*" EOS for the Al + SiC MMC [16].

These three types of EOS can be generalized using the so-called "*Mie-Gruneisen*" EOS [12], which can be written as:

$$P(\mu) = P_R(\mu) + \Gamma_R \rho_R (E(\mu) - E_R(\mu)) \tag{A.1}$$

where the compression $\mu = 1 - \rho_0/\rho$ and the subscript '*R*' is used to define the reference curves/quantities.

Shock EOS: In this case, the $P_R(\mu)$ and $E_R(\mu)$ are replaced with the corresponding Hugoniot curves, $P^H(\mu)$ and $E^H(\mu)$, which are in turn defined using a linear $U_s = C_0 + S\dot{x}$ relation (C_0 and S are material constants) as:

$$P^H(\mu) = \frac{\rho_R C_0^2 \mu(1+\mu)}{(1-(s-1)\mu)^2} \tag{A.2}$$

$$E^H(\mu) = \frac{1}{2}\frac{P^H}{\rho_R}\left(\frac{\mu}{1+\mu}\right) \tag{A.3}$$

Puff EOS: In this case the reference curves are again replaced with the respective Hugoniot curves. However, the latter are defined as:

$$P^H(\mu) = A_1\mu + A_2\mu^2 + A_3\mu^3 \tag{A.4}$$

$$E^H(\mu) = \frac{P^H}{\rho_R}\left(\frac{\mu}{2}\right) \tag{A.5}$$

where A_1, A_2 and A_3 are material constants and Eq. (A.5) is obtained Eq. (A.4) using the Rankine–Hugoniot relation.

Polynomial EOS: In this case, $h_R = P_R(\mu) - \Gamma_R\rho_R E_R(\mu)$ appearing in Eq. (A.1) is replaced with using a third order polynomial as

$$h_R = A_1\mu + A_2\mu^2 + A_3\mu^3 \tag{A.6}$$

Despite the fact that the Mie-Gruneisen EOS in the form of Eq. (A.1) is often used, its physical-basis is generally overlooked. Eq. (A.1) simply states that, if a reference curve defined by functions $P_R(\mu)$ and $E_R(\mu)$ and lying on the *P*-ρ-*E* EOS surface is known, the EOS surface can be reconstructed in the neighborhood of the reference curve by expanding each point of the curve, at a given of μ into a constant-μ line segment, so that the slope of this line segment is equal to Γ_R (the Gruneisen Gamma) material parameter.

A summary of the EOS material model parameters for the aluminum matrix, SiC reinforcements and the Al + SiC MMC is given in Table 1.

Appendix B. Dissipative pressure constitutive relation

As mentioned earlier, the dissipative-pressure/artificial-viscosity term Q is used to prevent excessive numerical oscillations by smearing the shock front over several computational cells/elements. Since the Q term is a remedy to the potential numerical problems, its partitioning between the composite-material constituents is not critical. For convenience, a zero value is often assigned to one of the constituents. Following Anderson et al. [11], the following constitutive relation is used in the present work:

$$Q = \rho k_1^2 \left(\frac{\dot{\rho}}{\rho}\right)^2 + \rho k_2 C_0 \left|\frac{\dot{\rho}}{\rho}\right| = \rho(q_q + q_l) \tag{B.1}$$

where k_1 and k_2 are material constants.

Clearly, since Q scales with $\dot{\rho}/\rho$, it can take significant values only in the shock front region where the rate of change of material density is significant. Also, within the finite-difference computational framework, Eq. (B.1) becomes:

$$Q^{n+(1/2)} = \rho^{n+(1/2)}(q_q + q_l) \tag{B.2}$$

It should be recalled that the Q-term for the homogenized material is related to the dissipative pressures of the individual components as $\rho Q\dot{\rho}/\rho = \rho_1 Q_1 \dot{\rho}_1/\rho_1 + \rho_2 Q_2 \dot{\rho}_2/\rho_2$, i.e. $Q\dot{\rho} = Q_1\dot{\rho}_1 + Q_2\dot{\rho}_2$.

Appendix C. Thermodynamic irreversibility-based temperature Hugoniot relations

The procedure described in this appendix enables calculation of the temperature Hugoniot arising from the irreversible nature of shock loading. As will be demonstrated below such calculation presumes the knowledge of the corresponding stress Hugoniot (or of the pressure Hugoniot in the hydrodynamic limit). The calculation procedure involves the following steps:

(a) First, the Rankine Hugoniot equation:

$$E^H(v) = E_R + 0.5(P^H(v) - P_R)(v_R - v) \tag{C.1}$$

is written in the differential form as:

$$\frac{dE^H(v)}{dv} = 0.5\left[(v_R - v)\frac{dP^H(v)}{dv} - P^H(v) - P_R\right] \tag{C.2}$$

(b) Then, the following expression for the combined first and second law of thermodynamics along the Hugoniot:

$$\frac{dE^H(v)}{dv} = \theta^H(v)\frac{d\eta^H(v)}{dv} - P^H(v) \tag{C.3}$$

(where η is a mass-based entropy density and θ is the absolute temperature) is combined with Eq. (C.2) to eliminate $dE^H(v)/dv$ to get:

$$\frac{d\eta^H(v)}{dv} = \frac{\kappa(v)}{2\theta^H(v)} \tag{C.4}$$

where $\kappa(v) = P^H(v) - P_R + (v_R - v)dP^H(v)/dv$.

(c)To obtain the temperature Hugoniot, $\theta^H(v)$, the $\eta^H(v)$ term must be eliminated from Eq. (C.4). Towards that end, the total derivative of the temperature is defined using the known thermodynamic derivatives [1] as:

$$d\theta = \left.\frac{\partial\theta}{\partial v}\right|_\eta dv + \left.\frac{\partial\theta}{\partial\eta}\right|_v d\eta = -\theta\frac{\Gamma(v)}{v}dv + \frac{\theta}{C(\eta)}d\eta \tag{C.5}$$

or

$$\frac{d\theta^H(v)}{dv} = -\frac{\Gamma(v)}{v}\theta^H(v) + \frac{1}{C^v(\eta^H(v))}\theta^H(v)\frac{d\eta^H(v)}{dv} \tag{C.6}$$

where Γ (the Gruneisen gamma) and C^v (the specific heat) are material-dependent parameters.

(d) Substitution of $d\eta^H(v)/dv$ from Eq. (C.4) into Eq. (C.6) gives

$$\frac{d\theta^H(v)}{dv} + \frac{\Gamma(v)}{v}\theta^H(v) = \frac{\kappa(v)}{2C_R^v} \tag{C.7}$$

Eq. (C.7) is a first order ordinary differential equation (ODE) in the quadrature format since its second term is a product of a function of the independent variable v and the dependent variable,

$\theta^H(v)$. These types of ODEs are integrals in a disguised form and can be readily integrated. On integration, Eq. (C.7) gives:

$$\theta^H(v) = \chi(v)\left[\theta_R + \frac{1}{2C_R^v}\int_{v_R}^{v}\frac{\kappa(v')}{\chi(v')}dv'\right] \tag{C.8}$$

where $\chi(v) = \exp\left((\Gamma(v_R)/v_R)(v_R - v)\right)$. Clearly, in order to get the temperature Hugoniot, $\theta^H(v)$, using Eq. (C.8), the pressure Hugoniot (i.e. the stress Hugoniot, in a general case) must be known.

Appendix D. Numerical procedure for shock analysis

In this section, a brief description is provided of the (explicit) incremental numerical procedure which was used in the present work to solve, as a function of time and a single spatial variable, the equations governing the propagation of planar shocks within two-phase composite materials. As mentioned earlier, in the case of a (two-component) composite material, the volume fractions of the two constituents are dynamic/state-dependent variables and, hence, are not known at the end of the new time increment. Hence, a (iterative) procedure has to be set up in order to compute simultaneously one of the constituent material's volume fraction (e.g. ϕ_1) and the remaining eight state variables ρ, $\dot{x}$, E_1, E_2, P_1, P_2, Q_1 and Q_2. As mentioned earlier, no thermal energy exchange is assumed to take place between the two phases residing within the same material point and, hence, the numerical procedure described below is strictly applicable only under this adiabatic condition.

The starting point in this case is the total-pressure equality condition, Eq. (20). After the appropriate EOS (Eqs. (A.2) and (A.4)) and Q_i (Eq. (B.1)) relations are plugged in to this equation, the resulting modified Eq. (20) defines a single equation with four unknowns: E_1, $\bar{\rho}_1$, E_2, and $\bar{\rho}_2$. Due to the adiabatic condition assumed, separate energy conservation equations, Eqs. (23) and (24) are used. After the energy rate in Eqs. (23) and (24) is expressed using a backward difference form and this equation is plugged in to the modified Eq. (20), one obtains a single equation with three unknowns, $\phi_1 = 1 - \phi_2$, $\bar{\rho}_1$, and $\bar{\rho}_2$. Two of these unknowns, $\bar{\rho}_1$ and $\bar{\rho}_2$, can be eliminated using the mass-fraction constancy condition $\gamma_i = \rho_i/\rho$, and the mass-density mixture equation, Eq. (16). The resulting relation is a single non-linear algebraic equation with one unknown, ϕ_1, which can be readily solved using the Newton–Raphson iterative procedure. The remaining dependent variables can then be obtained by back substitution.

References

[1] A.B. Pandey, K.L. Kendig, T.J. Watson, Proceedings of the TMS Materials Symposium, Indianapolis, USA, November, 2001.
[2] I. Lee, Y. Ochi, S. Bae, J. Song, Journal of Solid Mechanics and Materials Engineering 3 (7) (2009) 931–942.
[3] R.K. Abu Al-Rub, International Journal of Multi-scale Computational Engineering 7 (4) (2009) 329–350.
[4] P. Dang, M. Grujicic, Journal of Materials Science 32 (1997) 4875–4887.
[5] J.R. Davis, Aluminum and Aluminum Alloys, fifth ed., ASM International, 1993.
[6] E. Hunt, P.D. Pitcher, P.J. Gregson, Preparation Reactions in 8090 Particulate Reinforced MMCs, Technical Report ADA230646, Royal Aerospace Establishment, U.K., 1990.
[7] J.R. Davis, Heat Resistant Materials, second ed., ASM International, 1997.
[8] Y. Li, K.T. Ramesh, E.S.C. Chin, Journal of Composite Materials 41 (1) (2007) 27–40.
[9] K.S. Vecchio, G.T. Gray, Journal de Physique III 4 (1994), C8-231-236.
[10] D.S. Drumheller, International Journal of Impact Engineering 5 (1987) 261–268.
[11] C.E. Anderson, P.E. O'Donoghue, D. Skerhut, Journal of Composite Materials 4 (1990) 1159–1178.
[12] L. Davison, Fundamentals of Shock Wave Propagation in Solids, Springer-Verlag, Berlin/Heidelberg, 2008.
[13] R.A. Toupin, B. Bernstein, Journal of Acoustic Society of America 33 (1961) 216–225.
[14] M. Grujicic, Work in progress, 2011.
[15] B.S. Rao, V. Jayaram, Journal of Materials Research 16 (10) (2001) 2906–2913.
[16] ANSYS/Autodyn-2D and 3D, Version 11, User Documentation, ANSYS Inc., 2007.
[17] CES Selector, Version 4.6, Granta Design Limited, 2005.
[18] R. Becker, International Journal of Plasticity 20 (2004) 1983–2006.
[19] T.J. Vogler, J.D. Clayton, Journal of Mechanics and Physics of Solids 56 (2008) 297–335.